The 2009 IEEE/RSJ International Conference on
Intelligent Robots and Systems
October 11-15, 2009 St. Louis, USA

Development of an Exoskeleton Haptic Interface for Virtual Task Training

Craig Carignan, Jonathan Tang, and Stephen Roderick

Abstract— **An exoskeleton haptic interface is developed for functional training in virtual environments. A composite control scheme enables a variety of tasks to be implemented, and a "Qt" graphics library is used to generate the virtual environment for the haptic interface at the hand and graphical user interfaces for input and telemetry. Inter-process communications convert telemetry from the exoskeleton into motion commands for objects in the virtual environment. A second haptic interface at the upper arm is used to control the elbow orbit self-motion of the arm during tasks. Preliminary results are reviewed for a wall-painting task in which the virtual wall stiffness and viscosity are generated using an admittance controller.**

I. INTRODUCTION

The combination of virtual reality graphics with robotic force-feedback provides a powerful new tool for virtual reality (VR) training. In this scenario, simulated tasks with selectable parameters are generated on a computer display while the exoskeleton provides haptic (force) feedback in response to the subject's movement. A force sensor located at the hand gripper senses the forces being exerted by "contact" with the virtual environment, and the controller issues commands the exoskeleton in response to the interaction.

Exoskeletons provide significant advantages over other forms of robotics, particularly in rehabilitation applications. Since they surround the whole arm or leg, their motion naturally follows the subject. In addition, they can physically support the limbs during therapy, allowing a more seamless transition between assistive and resistive rehabilitation as a patient progresses.

The Maryland-Georgetown-Army (MGA) Exoskeleton, shown in Fig. 1, is a six degree-of-freedom (DOF) device designed primarily for shoulder rehabilitation. The shoulder assembly consists of three intersecting-axis rotary joints mounted on circular links surrounding the shoulder that replicates a "ball-and-socket" joint. In addition, a scapula joint mounted on the torso is used to replicate the shoulder elevation and depression that occurs as the result of tilting of the scapula joint about the thorax [1]. Other exoskeleletons, such as *ARMin II* [9] and *EXARM* [12], also incorporate various degrees of shoulder translation in their designs.

Several rehabilitation exoskeletons built to-date have incorporated virtual reality techniques in their protocol regimen. *L-Exos* built by PERCRO in Italy is a 5-DOF exoskeleton that can cover the full range of motion of the human arm [6]. A reaching task was generated using XVR graphics consisting of several moving spheres that needed to be grasped by subjects. Clinical trials on a group of nine post-stroke subjects resulted in significant improvements in reaching performance [7].

Fig. 1. The MGA Exoskeleton has six degrees of freedom and force/torque sensors mounted on both the upper arm and handle.

The *ARMin*, developed by ETH in Switzerland, is a rehabilitation arm exoskeleton that has 3 DOFs in the shoulder and 1 DOF at the elbow [11]. A game therapy experiment was generated in which a ball was dropped in a virtual environment and the subject had to "catch" the ball. In trials conducted with hemiplegic and spinal cord injury patients, motor functions were improved as noted by decreased reliance on robot support, increased range of motion of the upper limb, and increased motor coordination.

Due to its high torque capacity and control bandwidth, the MGA Exoskeleton can be used for either orthopedic rehabilitation or neuro-rehabilitation via functional training. A flexible control architecture based on composite patterns also allows different combinations of joints to be commanded to achieve multiple objectives. The kinematic design of the exoskeleton is first described in Section II, and then the modular control approach is described in Section III. The development of the graphical interfaces for a virtual wall-painting task are described in Section IV along with preliminary experimental results. Discussion of the results and plans for future work are outlined in Section V.

This work was supported by the U.S. Army Telemedicine and Advanced Technology Research Center (TATRC).

C. Carignan and J. Tang are with the Imaging Science and Information Systems Center, Georgetown University, Washington, DC 20057, USA crc32@georgetown.edu, jt96@georgetown.edu

S. Roderick is with the Space Systems Laboratory, University of Maryland, College Park, MD 20740, USA sroderick@umd.edu

II. MECHANICAL DESIGN

The kinematic configuration of the MGA Exoskeleton described in Denavit-Hartenberg (D-H) Notation is shown in Fig. 2 with resultant D-H parameter set given in Table I [5]. The first joint axis is mounted perpendicularly to the back and is used to realize elevation and depression of the shoulder. An orthogonal, intersecting-axis triad is used to generate the 3-axis rotation about the shoulder. The first shoulder axis is mounted at a 30° angle from vertical to rotate the singularity away from the vertical position (alignment of axes 1 & 3). The third shoulder axis intersects the upper arm link at an angle of 45° (rather than being coincident) to increase the range of motion. A single pitch joint drives elbow flexion/extension, and a passive forearm roll joint aft of the gripper allows free forearm supination/pronation through rotation of the handle.

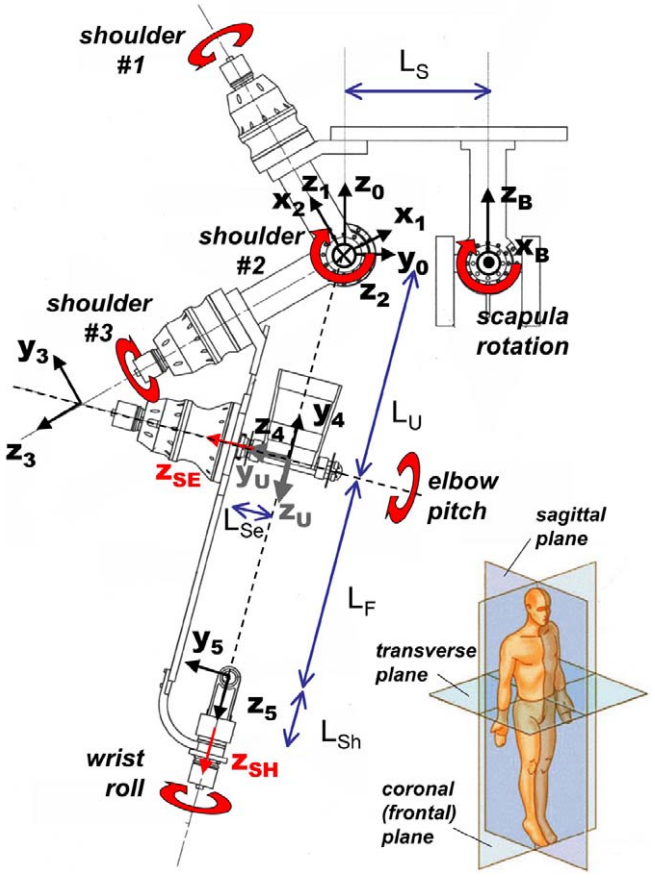

Fig. 2. D-H diagram of MGA Exoskeleton shown in the frontal (coronal) plane. Joint axes are along the z_i-axes, and links L_F, L_U, and L_S have adjustable lengths. The axial directions of the hand and elbow force sensors are represented by z_{SH} and z_{SE}, respectively. The body planes are shown in the inset (http://en.wikipedia.org/wiki/Image:BodyPlanes.jpg).

The schematic in Fig. 3 illustrates the resulting articulation of the MGA Exoskeleton. The scapula joint 0 located at B rotates the shoulder S along an arc of radius $\overline{BS}$. Joints 1-3 permit 3-axis rotation about the shoulder glenohumeral joint located at S. Joint 4 generates elbow flexion/extension. Finally, a rotary joint 5 located at the gripper permits passive forearm rotation about line $\overline{EW}$. The joint ranges allow the human arm almost complete freedom of movement within its workspace although shoulder abduction and flexion are somewhat more restricted [4].

TABLE I
D-H PARAMETERS FOR THE MGA EXOSKELETON.

link i	a_{i-1} (cm)	α_{i-1} (deg)	d_i (cm)	θ_i* home (deg)
1	0	$+30$	0	$+90$
2	0	-90	0	-105
3	0	$+90$	$\sqrt{2}L_U$	-90
4	0	-45	$-L_U$	0
5	0	-90	L_F	0

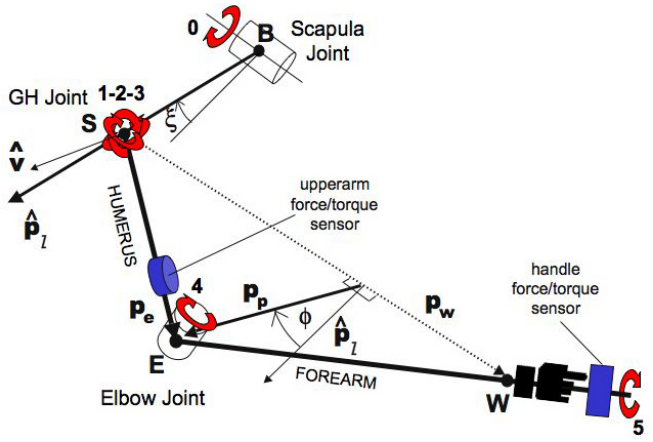

Fig. 3. Schematic representation of MGA Exoskeleton showing four anatomical joint groups and location of the force sensors.

A JR3, Inc. 50M31A force sensor is used to measure forces and torques at the handle, and a JR3 67M25 is mounted between the upper arm cuff and link to determine shoulder torques (see Fig. 4). The sensors are rated for 50 lb (25 lb) in the radial (axial) direction and are equipped with integrated sensor electronics. The six-channel digital output is read by a PCI card inside a PC at 8 KHz.

The linkages and actuator housings are constructed primarily from 6061 aluminum (Al) alloy, with some segments constructed from Al 2024 for increased stiffness. The scapula, upper arm, and forearm links contain passive prismatic joints to accommodate variable subject geometry: $L_S = 14.0-25.6$ cm, $L_U = 27.3 - 31.3$ cm, and $L_F = 30.0 - 39.0$ cm. The total mass of the exoskeleton is 11 kg, with the 1 kg actuator modules accounting for nearly half of the weight.

To simplify the forward kinematics, the base frame was chosen to be frame $\{0\}$ rather than frame $\{B\}$ due to the complexity introduced by the 30° skew angle between the z_0 and z_1 axes. Frame $\{B\}$ is then defined as a $-\theta_0$ rotation of the scapula joint about the x_0-axis from frame $\{0\}$ resulting in the translation ${}^B p_0$ and rotation ${}^B R_0$ relative to the base frame. The transformations between the base, handle, and body frames can then be cascaded to determine the position and orientation of the handle with respect to the body frame as follows:

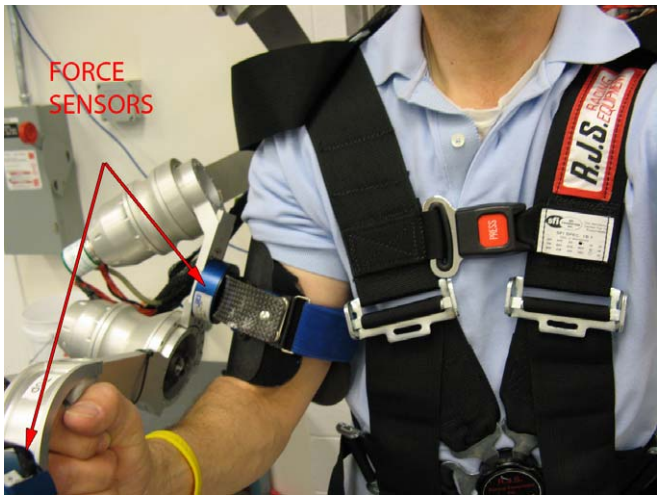

Fig. 4. A close-up of the MGA Exoskeleton showing the (blue) force-sensors mounted on the upper arm and wrist.

$$^{B}R_5 = {}^{B}R_0\,{}^{0}R_5 \quad (1)$$

$$^{B}p_5 = {}^{B}p_0 + {}^{B}R_0\,{}^{0}p_5 \quad (2)$$

The forward kinematics from joint 0 to joint 5, $^0p_5$ and $^0R_5$, are found by first finding the local link position and rotation transforms, $^ip_{i+1}$ and $^iR_{i+1}$ using the D-H parameters from Table I. These transforms are then cascaded to find the position $^0p_5$ and orientation $^0R_5$ of the handle with respect to the base frame [5].

Exoskeleton motion can still occur when the position of the hand and scapula are held fixed. This "self-motion" represents the ability of the elbow to "orbit" about the shoulder-wrist $\overline{SW}$ shown in Fig. 3. The elbow orbit angle ϕ is defined as the angle that the plane formed by the points S, E, and W makes with the reference plane defined by the reference vector, $\hat{v}$, and the shoulder-wrist vector, p_w [8]. Define the wrist and elbow vectors as $p_w \equiv {}^0p_5$ and $p_e \equiv {}^0p_4$, respectively, and let $\hat{v}$ denote an arbitrary fixed unit reference vector. The "elbow orbit angle" is then defined as the angle between p_p and p_ℓ

$$p_p \equiv p_e - \hat{p}_w(\hat{p}_w^T p_e) \quad (3)$$

$$p_\ell \equiv (p_w \times \hat{v}) \times p_w \quad (4)$$

$$tan\phi = \frac{\hat{p}_w^T(p_\ell \times p_p)}{p_\ell{}^T p_p} \quad (5)$$

Since the elbow orbit angle is a rather complex function of the arm angles, ϕ is more easily computed by performing the numerical vector operation in (5) and then taking the arctangent of the result.

III. CONTROL SYSTEM

Because the exoskeleton is kinematically redundant with respect to hand position, a second haptic interface is required in addition to the gripper. This additional interface is located at the arm cuff that connects the humerus to the upper arm link. For tasks that are dominated by hand placement, the arm cuff interface is used to control the torque that produces the arm self-motion. For example, during a reaching task, this interface can be used to enforce proper shoulder abduction, which is often absent in stroke patients [14]. During shoulder exercises, such as shoulder abduction or flexion, the arm cuff becomes the primary haptic interface that controls shoulder rotation [2].

To accommodate multiple haptic interfaces and an extra scapula joint, a "composite" control architecture was developed that is capable of controlling different sets of exoskeleton joints concurrently [3]. For example, in shoulder rotation exercises, the three shoulder glenohumeral (GH) joints are controlled as one group (GH) while the scapula (SC) and elbow (EP) joints are controlled independently. In functional tasks involving whole arm motion, the shoulder and elbow joints are controlled together (XW) because they both determine hand position and elbow orbit, and then the scapula joint (SC) is controlled independently.

Each subcontroller can operate in impedance, admittance, or position mode, which issues either position or torque commands to the joint servos. If motion dominates the dynamic behavior at the haptic interface, then the exoskeleton functions as the impedance device moving in response to the forces exerted by the subject. If the contact forces are dominant at the haptic interface, then the exoskeleton acts as the admittance device and the sensed forces at the handle (or upper arm) are used to drive its motion.

An example of a valid composite control realization for a whole arm task invokes two sub-controllers as shown in Fig. 5: scapula (Sc) position control for joint 0 and wrist translation/elbow orbit control (XW) for joints 1-4. The wrist translation and elbow orbit motion are co-dependent on the four arm joint angles and are either determined by force or position input from the operator. A position controller is used to independently drive the scapula joint as a function of the upper arm elevation. The subcontrollers that were used in the wall-painting experiment are described below.

A. Wrist/Elbow Admittance Module

The admittance controller shown in Fig. 6 is used to convert the sensed contact forces at the handle and elbow orbit torque into desired movements of the exoskeleton. Force signals at the hand are relayed to an admittance model of the virtual environment, which then outputs a desired velocity for the wrist, $\dot{p}_w$. The z-component of the elbow force sensor in f_{S_e} is used to determine the torque, τ_ϕ, exerted about the shoulder-wrist axis, p_w. The elbow orbit torque is calculated by taking the product of the the z-component of the force multiplied by the moment arm

$$\tau_\phi \equiv \mid p_p \mid f_{S_e} \bullet \hat{z} \quad (6)$$

where p_p is the minimum distance from the elbow to $\overline{SW}$.

The inverse kinematics for the arm joint angles θ_a are found from $^0p_5$ and ϕ using the extended Jacobian approach [13]. Because of the complex dependence of the

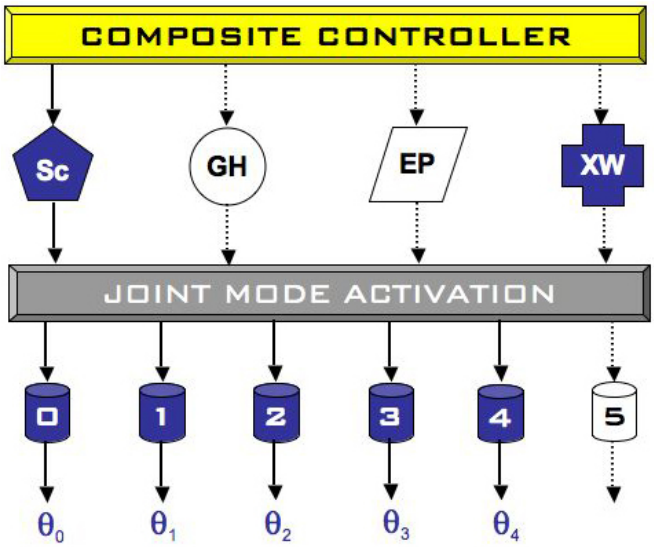

Fig. 5. A composite control realization for a whole arm task, where the Sc subcontroller outputs a scapula position command and the XW admittance subcontroller outputs shoulder/elbow joint position commands.

wrist position and, in particular, the elbow orbit angle on the joint angles, an analytical solution for the exoskeleton inverse kinematics is not realizable. Thus, a Newton-Raphson iterative procedure is used to determine the change in joint angles as a function of the desired change in wrist position and elbow orbit angle.

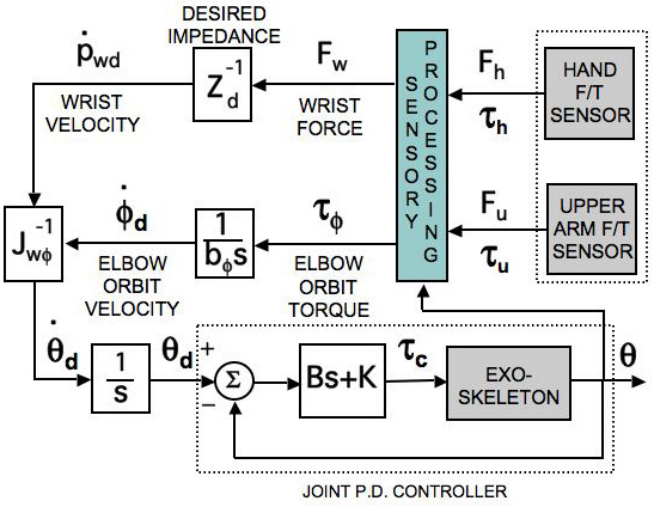

Fig. 6. The admittance controller utilizes force inputs from the force sensors mounted on the upper arm and handle to compute the desired wrist velocity and elbow orbit angular rate, which are then input to the inverse kinematics to determine the exoskeleton joint rates.

B. Scapula PD Module

Maintaining the center of rotation of the exoskeleton and human shoulder joints is important because misalignment stresses can cause discomfort, pain, and possibly even damage to the shoulder under repetitive motion [11]. Thus the exoskeleton's scapula joint is commanded to follow a biomechanical model of the motion of the human's glenohumeral (GH) joint as the upper arm elevates. Data of GH motion from [10] was used to generate curve fits for the GH vertical displacement Δy as a function of the humerus elevation ξ, where $\Delta y = 0$ represents the shoulder elevation when the arm is extended horizontally at 90° [4]. Since the z-axis of the upper arm frame $\{U\}$ is directed along the humerus, the humerus elevation can be obtained from the dot product of the z-axis of frame $\{U\}$ with the z-axis (azimuth) of the body frame $\{B\}$, i.e. the (3,3) element of ${}^{B}R_{U}$

$$\xi = 180° - cos^{-1}({}^{B}R_{U_{3,3}}) \tag{7}$$

where $\xi = 0°$ when the humerus is vertical against the side of the trunk. Thus the desired scapula angle is obtained from

$$\theta_0 = tan^{-1}(\Delta y / L_S) \tag{8}$$

where the scapula link length L_S is adjusted to be the length of the clavicle (≈15 cm for the average adult male [4]).

IV. WALL PAINTING EXPERIMENT

An architectural overview of the control system is shown in Figure 7. The control station runs a Mac OS X operating system and implements a set of graphical interfaces written in Trolltech Qt 4 to select protocols, initiate/terminate operation, and monitor subject data. The control station communicates over the Internet with the robot control computer, which is used to execute the main control loop and safety monitoring system. The robot control computer runs a TimeSys6 Linux real-time operating system at 125 Hz to ensure safety deadlines. A dual channel PCI card in the robot control computer processes strain gauge signals from the JR3 force sensors at 8 KHz and sends the resulting force data to the arm controllers.

Each joint is driven by a Kollmorgen brushless DC motor (RBE series) and harmonic drive transmission from HD Systems (CSF/CSD series). Communication and power are routed through an umbilical to a Galil DMC18x6 6-Axis motion control card running at 1000 Hz and B30A8 brushless servo amplifiers from Advanced Motion Control, Inc. Motor position is determined using a Numerik Jena 1800-line optical incremental encoder mounted to the motor shaft. Absolute 12-bit optical encoders from Gurley Precision Instruments (Model A37B) are mounted at the output of the transmission to determine absolution position on start up and to monitor the incremental encoders.

Qt was used to generate the virtual wall graphics seen in Fig. 8. An icon of a paintbrush is drawn on a plain background based on the Cartesian pose of the exoskeleton handle. Movement of the exoskeleton handle causes movement of the paintbrush in the graphical interface. When the roller makes contact with the wall, a bright green swath is painted along the surface. A bar graph is superposed on the wall to indicate the level of force to the user who attempts to keep it within a specified range.

The graphical user interface shown in Fig. 9 allows the clinician to input parameters for the wall-painting task.

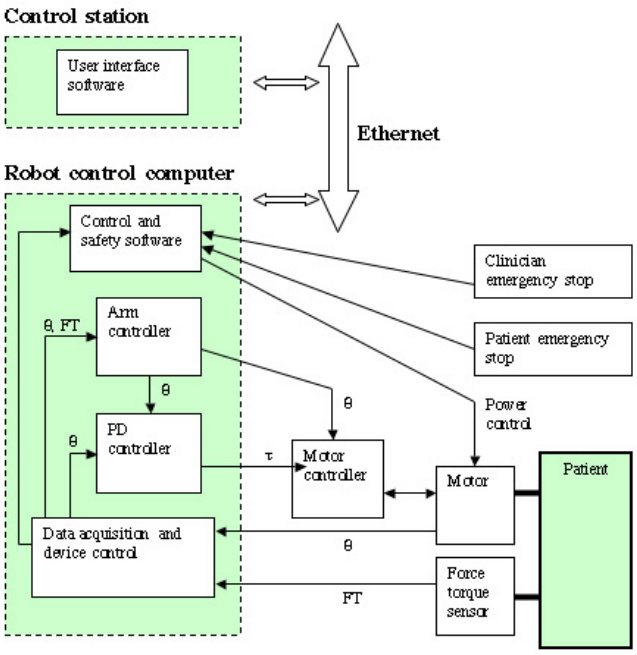

Fig. 7. Exoskeleton control system architecture.

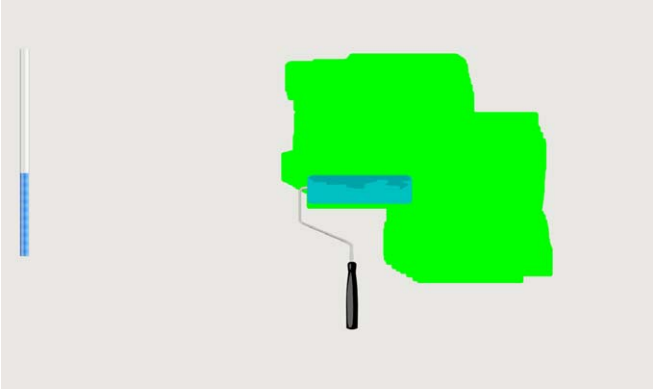

Fig. 8. Wall painting graphics developed using Qt 4.

Graphical icons are used to navigate the input space, allowing a more natural selection of the task parameters. The plane of the wall is chosen using radio buttons (coronal, transverse, or sagittal), and the wall distance is input using the boxes to the left. Wall, ceiling, and floor boundaries are chosen to restrict the workspace. Finally, the wall stiffness and damping parameters are chosen using sliders and buttons, or they can be input numerically in the boxes provided.

In the experiments, the stiffness of the wall was chosen to be 1500 N/m, and the damping was B=1500 N/m/s normal to the wall. In the directions tangent to the wall, stiffness was zero and damping was 100 N/m/s. The elbow orbit damping was chosen to be 50 N-m/rad/s. Since zero impedance is not realizable with an admittance controller, a finite damping value of 100 N/m/s was used in all directions in freespace.

A video snapshot of the experimental setup is shown in Fig. 10. The virtual wall is located in the Coronal plane at a distance of 0.4 m from the intersection of the body plane

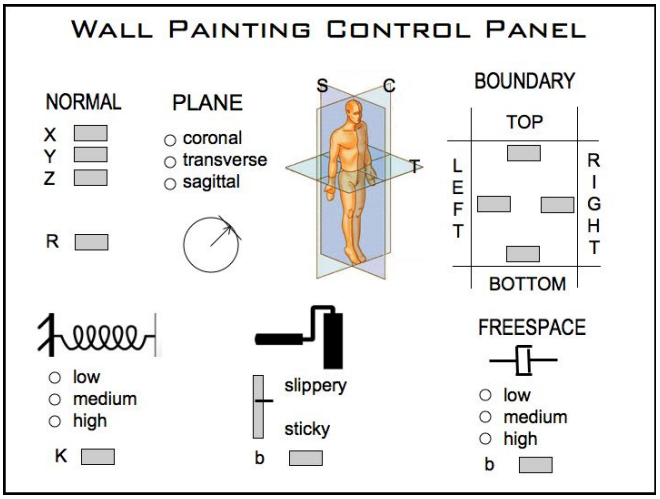

Fig. 9. Control GUI being developed for the wall-painting task allows selection of wall position, boundaries, and stiffness as well as viscosity of the roller brush on the wall surface.

axes. The subject starts with their hand a few centimeters in front of the wall and then moves forward until contact is made. The subject was told to hold a constant force on the surface, but the force level is not currently displayed. The force reached a peak of about 60 N for a 3 cm "deflection" of the wall surface as seen in Fig. 11.

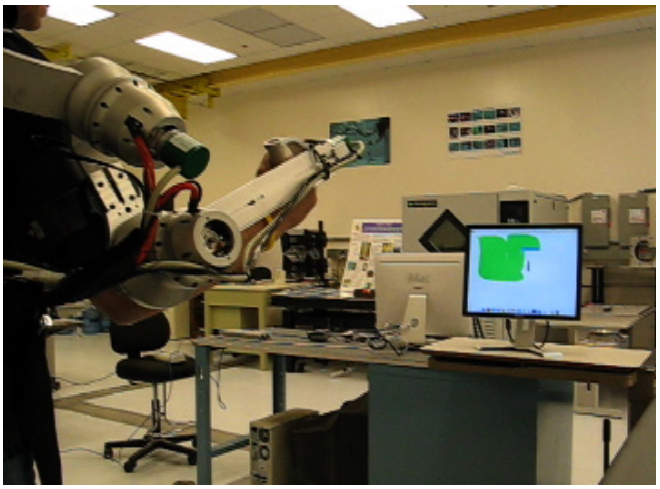

Fig. 10. Video capture of subject performing wall-painting task.

A 3D rendering of the hand path is shown in Fig. 12, where the color indicates the level of force exerted at each point. As can be seen, the force increase greatly past 0.4 m, which is the location of the wall. However, viscous damping also results in resistance even when the brush is not in contact with the virtual wall shown in Fig. 10. The wall stiffness was limited to about 2000 N/m by stability considerations in the admittance controller and requires nonzero damping impedances in all directions. This causes an unnatural simulation when the brush is lifted off the wall and moved to another location.

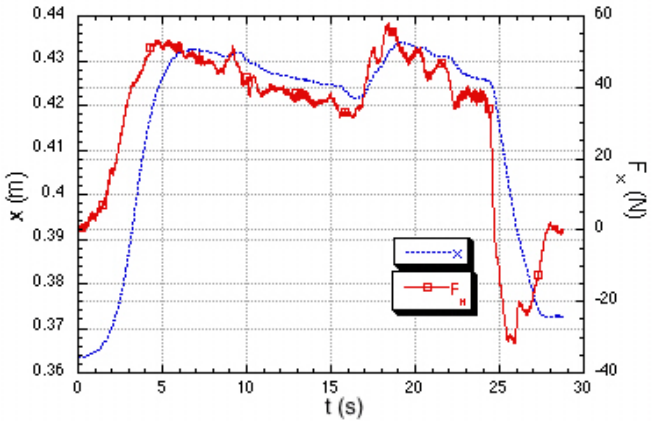

Fig. 11. Handle position and contact force normal to wall.

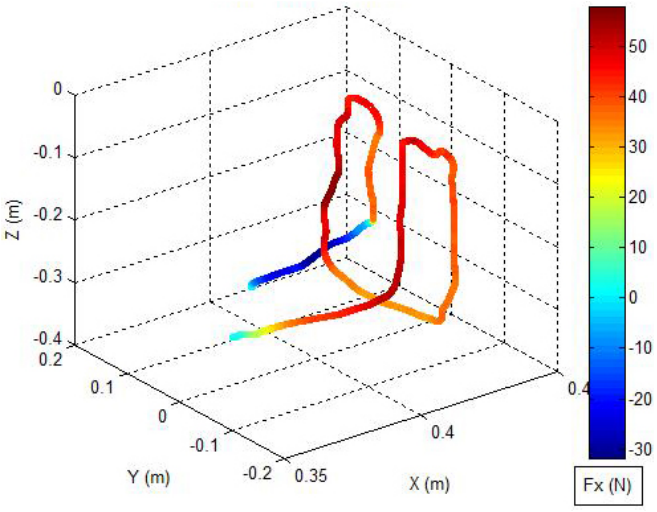

Fig. 12. Cartesian path of handle shown in 3D perspective. The color of the line indicates the level of force exerted normal to the wall.

V. CONCLUSION

The MGA Exoskeleton was used in conjunction with a Qt-generated virtual environment to create a simple wall-painting virtual task for rehabilitation. This task will allow the clinician to specify a desired range of forces to be applied to the virtual wall by the roller brush and cause the patient to abduct the shoulder in order to accomplish the task. The controller was able to replicate the desired wall stiffness and viscosity along the wall surface during the task.

An impedance controller is being developed that will allow low impedance simulations of the same task and zero impedance in freespace. Implementation of the impedance controller will require gravity and friction compensation to cancel out the dominant (non-inertial) dynamics of the exoskeleton at low accelerations. The link masses and joint frictions have been characterized for the compensation and are now being tested with the controller.

ACKNOWLEDGMENTS

Thanks go to Mike Liszka, Emmanuel Wilson, and Mike Perna for their engineering support. This project was sponsored by the U.S. Army Telemedicine and Advanced Technology Research Center under #W81XWH-08-2-0010.

REFERENCES

[1] D. G. Caldwell, C. Favede, and N. Tsagarakis, "Dextrous exploration of a virtual world for improved prototyping," in *Proc. of the IEEE Intl. Conf. on Robotics and Automation*, Leuven, Belgium, May 1998, pp. 298–303.

[2] C. Carignan, M. Naylor, and S. Roderick, "Controlling shoulder impedance in a rehabilitation arm exoskeleton," in *Proc. IEEE Int. Conf. on Robotics and Automation*, Noordwijk, Netherlands, May 2008, pp. 2453–2458.

[3] C. Carignan, S. Roderick, and M. Naylor, "Distributed control and safety system for a rehabilitation arm exoskeleton," in *ASME Int. Mechanical Engineering Congress and Exposition (IMECE)*, Seattle, Nov. 2007.

[4] C. Carignan, J. Tang, S. Roderick, and M. Naylor, "A configuration-space approach to controlling a rehabilitation arm exoskeleton," in *Int. Conf. on Rehabilitation Robotics (ICORR)*, Noordwijk, Netherlands, June 2007, pp. 179–187.

[5] J. Craig, *Introduction to Robotics: Mechanics and Control, 2nd ed.* Reading, Mass.: Addison-Wesley, 1989.

[6] A. Frisoli, F. Rocchi, S. Marcheschi, A. Dettori, F. Salsedo, and M. Bergamasco, "A new force-feedback arm exoskeleton for haptic interaction in virtual environments," in *Proc. of the First Joint Euro-haptics Conference and Symposium on Haptic Interfaces for Virtual Environment and Teleoperator Systems*, 2005, pp. 195–201.

[7] A. Frisoli, L. Borelli, A. Montagner, S. Marcheschi, C. Procopio, F. Salsedo, M. Bergamasco, M. C. Carboncini, and B. Rossi, "Robot-mediated arm rehabilitation in virtual environments for chronic stroke patients: a clinical study," in *Proc. IEEE Int. Conf. on Robotics and Automation*, Pasadena, 2008, pp. 2465–2470.

[8] K. Kreutz-Delgado, M. Long, and H. Seraji, "Kinematic analysis of 7 DOF manipulators," *Int. Journal of Robotics Research*, vol. 11, no. 5, pp. 469–481, 1992.

[9] M. Mihelj, T. Nef, and R. Riener, "ARMin II – 7 DOF rehabilitation robot: mechanics and kinematics," in *Proc. IEEE Int. Conf. on Robotics and Automation*, rome, 2007, pp. 4120–4125.

[10] T. B. Moeslund, C. B. Madsen, and E. Granum, "Modelling the 3D pose of a human arm and the shoulder complex utilising only two parameters," in *Proc. of the Intl. Conference on Model-based Imaging, Rendering, Image Analysis and Graphical Special Effects*, INRIA Rocquencourt, France, 2003, pp. 11–19.

[11] T. Nef, M. Mihelj, G. Kiefer, C. Pemdl, and R. Muller, "ARMin – exoskeleton for arm therapy in stroke patients," in *Proc. IEEE Int. Conf. on Rehabilitation Robotics*, Noordwijk, The Netherlands, 2007, pp. 68–74.

[12] A. Schiele and G. Visentin, "The ESA human arm exoskeleton for space robotics telepresence," in *Proc. 7th Int. Symposium on Artificial Intelligence, Robotics and Automation in Space (iSAIRAS)*, Nara, Japan, 2006.

[13] H. Seraji, "Configuration control of redundant manipulators: Theory and implementation," *IEEE Transactions on Robotics and Automation*, vol. 5, no. 4, pp. 472–490, Aug. 1989.

[14] T. Sukai, M. Ellis, and J. Dewald, "Shoulder abduction-induced reductions in reaching work area following hemiparetic stroke," *Experimental Brain Research*, vol. 183, pp. 215–223, 2007.